Size and speed of the working stroke of cardiac myosin in situ

Marco Caremani[a], Francesca Pinzauti[a], Massimo Reconditi[a,1], Gabriella Piazzesi[a], Ger J. M. Stienen[b,c], Vincenzo Lombardi[a,2], and Marco Linari[a]

[a]Laboratory of Physiology, Department of Biology, Università di Firenze, 50019 Sesto Fiorentino, Florence, Italy; [b]Department of Physiology, Institute for Cardiovascular Research, VU University Medical Center, 1081 HV Amsterdam, The Netherlands; and [c]Department of Physics and Astronomy, Faculty of Science, VU University, 1081 HV Amsterdam, The Netherlands

Edited by James A. Spudich, Stanford University School of Medicine, Stanford, CA, and approved February 19, 2016 (received for review December 18, 2015)

The power in the myocardium sarcomere is generated by two bipolar arrays of the motor protein cardiac myosin II extending from the thick filament and pulling the thin, actin-containing filaments from the opposite sides of the sarcomere. Despite the interest in the definition of myosin-based cardiomyopathies, no study has yet been able to determine the mechanokinetic properties of this motor protein in situ. Sarcomere-level mechanics recorded by a striation follower is used in electrically stimulated intact ventricular trabeculae from the rat heart to determine the isotonic velocity transient following a stepwise reduction in force from the isometric peak force T_P to a value T (0.8–0.2 T_P). The size and the speed of the early rapid shortening (the isotonic working stroke) increase by reducing T from ∼3 nm per half-sarcomere (hs) and 1,000 s^{-1} at high load to ∼8 nm·hs^{-1} and 6,000 s^{-1} at low load. Increases in sarcomere length (1.9–2.2 μm) and external $[Ca^{2+}]_o$ (1–2.5 mM), which produce an increase of T_P, do not affect the dependence on T, normalized for T_P, of the size and speed of the working stroke. Thus, length- and Ca^{2+}-dependent increase of T_P and power in the heart can solely be explained by modulation of the number of myosin motors, an emergent property of their array arrangement. The motor working stroke is similar to that of skeletal muscle myosin, whereas its speed is about three times slower. A new powerful tool for investigations and therapies of myosin-based cardiomyopathies is now within our reach.

cardiac myosin | myosin working stroke | heart mechanics

The performance of heart depends on the power developed by the myocardium, which in turn is strongly dependent on the end-diastolic volume modulating the systolic pressure development (Frank–Starling law of the heart). At the level of the sarcomere, the structural unit of striated muscle, the Frank–Starling law originates from the increase in the force of contraction with an increase in sarcomere length (length-dependent activation). Mutations of sarcomere proteins affect power output and are considered responsible for various forms of cardiomyopathy (1, 2). Over 250 mutations in cardiac myosin II have been reported as the cause of cardiomyopathies (1, 3, 4). Defining the mechanokinetic properties of the cardiac myosin in situ is therefore fundamental to understand the pathomechanisms of these cardiomyopathies and to provide previously unidentified therapeutic opportunities.

In the sarcomere, the myosin motors are organized in two bipolar arrays extending from the thick filament and pulling the thin actin-containing filaments from the opposite sides of the sarcomere toward its center. In each array, the myosin motors are connected in parallel via their attachments to the thick filament and the resulting collective motor provides steady force and shortening by cyclic asynchronous ATP-driven actin–myosin interactions. Thus, the performance of the heart relies on the integration of the mechanokinetic properties of the myosin motor and the properties emerging from its array arrangement in the half-sarcomere (hs). Using sarcomere-level mechanics in intact cells from the skeletal muscle, it has been shown that the isotonic velocity transient following stepwise changes in force imposed on the otherwise isometric contraction contains information on both the working stroke of the myosin motor and the steady-state force–velocity (T–V) relation resulting from the cyclic actin–myosin interactions and accounting for the power output (5–9).

Here, this approach is applied for the first time (to our knowledge) to a multicellular cardiac preparation like the intact trabecula dissected from the right ventricle of the rat heart. A striation follower (10) proved to be a reliable tool for measurement of sarcomere length changes with nanometer–microsecond resolution owing to optical averaging of the image of the sarcomeres that reduces the background noise originating from intracellular and intercellular components of the trabecula. Following the original idea by ter Keurs et al. (11), the sarcomere shortening recorded during the force development in a fixed-end twitch is used as a feedforward signal to maintain sarcomere length constant during the next twitch. By switching from length control to force control, a stepwise drop in force was imposed at the peak of force (T_P) to record the isotonic velocity transient. In this way, the amplitude and speed of the rapid phase of the transient (phase 2), which is the mechanical manifestation of the myosin working stroke, could be determined. Increases in sarcomere length (SL) from 1.9 to 2.2 μm and in the external Ca^{2+} concentration ($[Ca^{2+}]_o$) from 1 to 2.5 mM, which produce an increase in T_P, do not affect the myosin working stroke. This indicates that length-dependent potentiation of cardiac contractility is fully accounted for by an increase in the number of attached myosin motors. These experiments demonstrate that our sarcomere-level mechanical methods have the full potential for the in situ investigation of cardiomyopathy-causing mutations in cardiac myosin.

Results and Discussion

Force–SL Relation. The twitch in response to an electrical stimulus at the steady state of 0.5-Hz electrical pacing with 1 mM $[Ca^{2+}]_o$

Significance

To our knowledge, this paper represents a major advancement in the physiology and pathophysiology of the heart as it gives the first quantitative description of the working stroke of the motor protein cardiac myosin II. The experiments demonstrate that our sarcomere-level mechanical methods on trabeculae have the full potential for the in situ investigation of cardiomyopathy-causing mutations in cardiac myosin and tests on specific therapeutic interventions.

Author contributions: M.C., F.P., M.R., G.P., G.J.M.S., V.L., and M.L. designed research; M.C., F.P., M.R., G.P., G.J.M.S., and M.L. performed research; M.C., F.P., and M.R. analyzed data; and G.P., G.J.M.S., V.L., and M.L. wrote the paper.

The authors declare no conflict of interest.

This article is a PNAS Direct Submission.

[1]Present address: Department of Experimental and Clinical Medicine, Università di Firenze, 50134 Florence, Italy.

[2]To whom correspondence should be addressed. Email: vincenzo.lombardi@unifi.it.

This article contains supporting information online at www.pnas.org/lookup/suppl/doi:10.1073/pnas.1525057113/-/DCSupplemental.

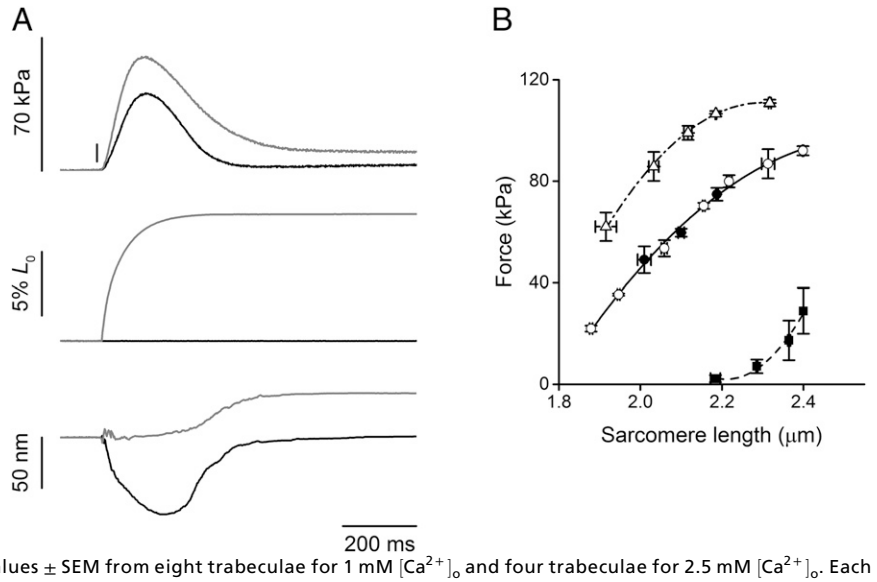

Fig. 1. Force developed in a twitch and its relation with SL. (*A*) Force development upon electrical stimulation at 0.5 Hz and 1.0 mM $[Ca^{2+}]_o$, during fixed-end (black trace) and isometric-sarcomere conditions (gray trace) at an initial SL of 2.2 μm. Upper trace, force; middle trace, motor position; lower trace, hs length change. The isometric-sarcomere force development is obtained by the feedforward lengthening imposed on the trabecula as detailed in the text and prevents sarcomere shortening during force development. The bar on the force trace marks the stimulus start. Length of the trabecula, 3.35 mm; segment length under the striation follower, 1.28 mm; average SL, 2.18 μm; cross-sectional area, 26,700 μm^2; temperature, 27.2 °C. (*B*) Relations between peak force (T_P) and SL at 1 mM $[Ca^{2+}]_o$ (active force, circles; passive force, squares) and 2.5 mM (active force, triangles). The lines are polynomial fits to data. The relation between active force and SL obtained in fixed-end conditions (filled circles) does not differ from that under sarcomere-isometric conditions (open circles) in which the initial SL shortening was prevented by the feedforward method. Mean values ± SEM from eight trabeculae for 1 mM $[Ca^{2+}]_o$ and four trabeculae for 2.5 mM $[Ca^{2+}]_o$. Each point is the average of three to eight data points from different trabeculae.

in fixed-end conditions is shown in Fig. 1*A* (black trace). During force development (*Upper*), sarcomeres shorten against the compliant end regions by 80 nm per hs (*Lower*), corresponding to 7.3% L_0. This internal shortening was prevented in the next twitch (gray trace) by feeding the summing point of the motor servo-system with an equivalent inverted signal (*Middle*). The peak force (T_P) attained in these sarcomere-isometric conditions was considerably larger (30%) than that attained under fixed-end conditions, while the sarcomere shortening was completely prevented (*Lower*). The relation between T_P and SL (range, 1.9–2.4 μm) obtained in 1 mM $[Ca^{2+}]_o$ is shown in Fig. 1*B* (circles). The plotted data indicate T_P after subtraction of the passive force (squares) that starts to rise at SL >2.15 μm (see also Fig. S1). It can be seen that data from fixed-end conditions (filled circles) lie on the same relation as those in sarcomere-isometric conditions (open circles). Thus, there is a unique relation between peak force and SL, independently of the shortening undergone during force rise. At SL of 2.3 μm, T_P reaches a value of 87 ± 6 kPa (mean ± SEM), almost twice the value at SL of 2.0 μm. These results agree with the original study by ter Keurs et al. (11), who used laser diffraction to record and clamp SL.

The rise in $[Ca^{2+}]_o$ to 2.5 mM increases T_P at any SL, so that the relation is shifted upward (triangles). Actually, the two curves do not run parallel, because with $[Ca^{2+}]_o$ of 2.5 mM the relation is more concave, apparently reaching a force maximum at SL of 2.3 μm (see also ref. 11).

Isotonic Velocity Transients. The isotonic velocity transient was elicited by superimposing, on the peak force of an otherwise isometric contraction at 1 mM $[Ca^{2+}]_o$, a stepwise drop in force from T_P to a value in the range of 0.2–0.8 T_P. Fig. 2 *A* and *B* show the isotonic velocity transient in response to a drop in force to 0.5 T_P from a typical experiment at SL of 2.2 μm. Several phases could be distinguished, named after those first described in single fibers from frog skeletal muscle (8, 12): phase 1, a shortening simultaneous with the drop in force, due to the hs elasticity; phase 2, the early rapid shortening, which is attributed to the synchronous execution of the working stroke in the attached myosin motors; phase 4, the late steady shortening at constant velocity due to cyclic detachment-reattachment of motors. Apparently, in contrast to skeletal muscle, there is not a pause (phase 3) in shortening between the end of phase 2 and beginning of phase 4.

The merging between the end of the elastic shortening (phase 1) and the early rapid shortening (phase 2) might result in an overestimation of the elastic response at the expenses of the working stroke response (8). Therefore—as illustrated in Fig. 2*C* (for a force drop to 0.75 T_P) and Fig. 2*D* (same record as Fig. 2*A*)—to estimate the size of phase 1 (L_1), the contribution of phase 2 to phase 1 is subtracted by back-extrapolating, to the force step half-time ($t_{1/2}$, vertical dashed line), the tangent to the initial part of phase 2 (magenta line). Phase 2 following the elastic response has a nearly exponential time course and its size can be estimated by subtracting, from the length trace, the linear back extrapolation of the phase 4 shortening trace to $t_{1/2}$ (green line in Fig. 2 *C* and *D*). The distance between the horizontal trace obtained with the subtraction procedure and the length before the step (Fig. 2*E*, from the same record as in Fig. 2*A*) estimates the total amount of shortening at the end of phase 2 (L_2). The difference ($L_2 - L_1$) estimates L_T, the amount of shortening accounted for by the working stroke of the myosin motors at the force *T*. Assuming an exponential time course of phase 2 shortening, the time elapsed between $t_{1/2}$ and the abscissa intercept of the tangent to the initial part of the trace (magenta line) is an estimate of the time constant of phase 2 shortening and its reciprocal is an estimate of the rate constant of the process (r_2). r_2 can be estimated also by fitting the shortening trace with an exponential starting from the end of the imposed force step (green dashed line in Fig. 2*E*, and Fig. S2). As shown in the table in Fig. S2, the two methods gave similar results and the value of r_2 obtained with the exponential fit has been used throughout the paper.

After the elastic phase 1 response occurring during force drop, the rest of shortening transient occurs at constant force and thus is independent of the amount of series compliance. In fact, as shown in Fig. 2*F* (from the same record as Fig. 2*A*), the phase 2 shortening obtained as described above from the position of the motor hook (motor lever position, red dashed trace) perfectly superimposes on that obtained from the SL signal (*L*, black trace).

L_1 (triangles) and L_2 (circles) dependence on *T* is shown in Fig. 3*A*. L_T calculated from these data (open circles in Fig. 3*B*) and L_T estimated from the motor lever position signal show the same dependence on *T*.

The results pooled from the eight trabeculae analyzed at SL of 2.2 μm and 1 mM Ca^{2+} are shown by the open symbols in Fig. 3*C*. L_T increases with the reduction of *T* from 3 nm·hs^{-1} at 0.8 T_P to 8 nm·hs^{-1} at 0.2 T_P. The intercept on the ordinate of the linear fit (continuous line) to the L_T data (the size of the working stroke at zero load) is 9.7 ± 0.3 nm. r_2 increases with the reduction of the

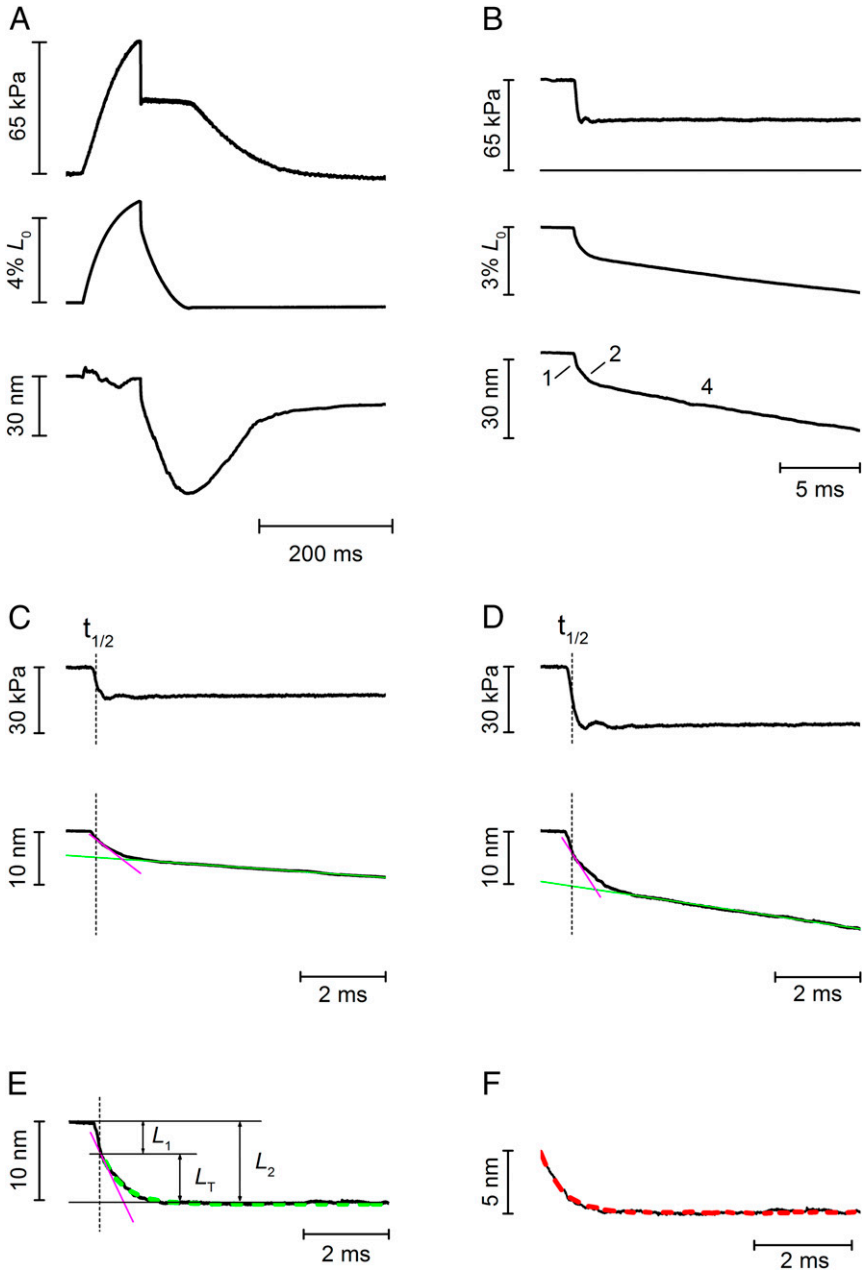

Fig. 2. Isotonic velocity transients following a stepwise drop in force. (*A*) Shortening of the hs (lower trace) in response to a step to 0.5 T_P superimposed on the force at a time just before the attainment of the peak force developed under sarcomere-isometric conditions (upper trace); middle trace, motor position. (*B*) Same shortening response as in *A* on a faster timescale. Numbers close to the shortening record identify the phases of the transient named after those first described in skeletal muscle (8). (*C* and *D*) Early components of the isotonic velocity transient to show the methods for estimating L_1 and L_2 (*C* in response to a step to 0.75 T_P, and *D* for the same record as in *A*). L_1 is measured by extrapolating the tangent to the initial part of phase 2 (magenta line) back to the half-time of the force step ($t_{1/2}$, indicated by the vertical dashed line). L_2 is measured by extrapolating the ordinate intercept of the straight line fitted to phase 4 shortening (green line in *C* and *D*, the slope of which measures the steady shortening velocity) back to $t_{1/2}$. (*E*) Time course of phase 2 shortening calculated by subtracting the green line fitted to phase 4 shortening from the overall shortening transient. L_T, the size of the isotonic working stroke, is obtained by subtracting the elastic response L_1 from L_2. The green dashed line is the exponential fit to the trace starting from the end of the force step (Fig. S2). (*F*) Superimposed SL signal (black) and motor lever signal (red dashed) after subtraction of phases 1 and 4. Length of the trabecula, 2.5 mm; segment length under the striation follower, 1.4 mm; average SL, 2.19 μm; cross-sectional area, 14,100 μm^2; temperature, 27.1 °C.

load (open symbols in Fig. 3*D*) from ~1,000 s^{-1} at 0.8 T_P to ~6,000 s^{-1} at 0.2 T_P.

Phase 2 evolves directly into the final steady shortening characteristic of the force–velocity relation (phase 4, open symbols in Fig. 4 *A* and *B*). The curvature (a/T_P= 0.33 ± 0.03) and the ordinate intercept (the unloaded shortening velocity, V_0 = 8.40 ± 0.25 μm/s per hs) of the relation are estimated by fitting the hyperbolic Hill equation to data.

The sliding velocity in phase 2 (V_2), estimated as the product of L_T times r_2, has also a hyperbolic dependence on T (Fig. 4*C*, blue open symbols). V_2 increases from ~3,000 nm/s per hs at 0.8 T_P to 50,000 nm/s per hs at 0.2 T_P. Thus, as in frog muscle fibers

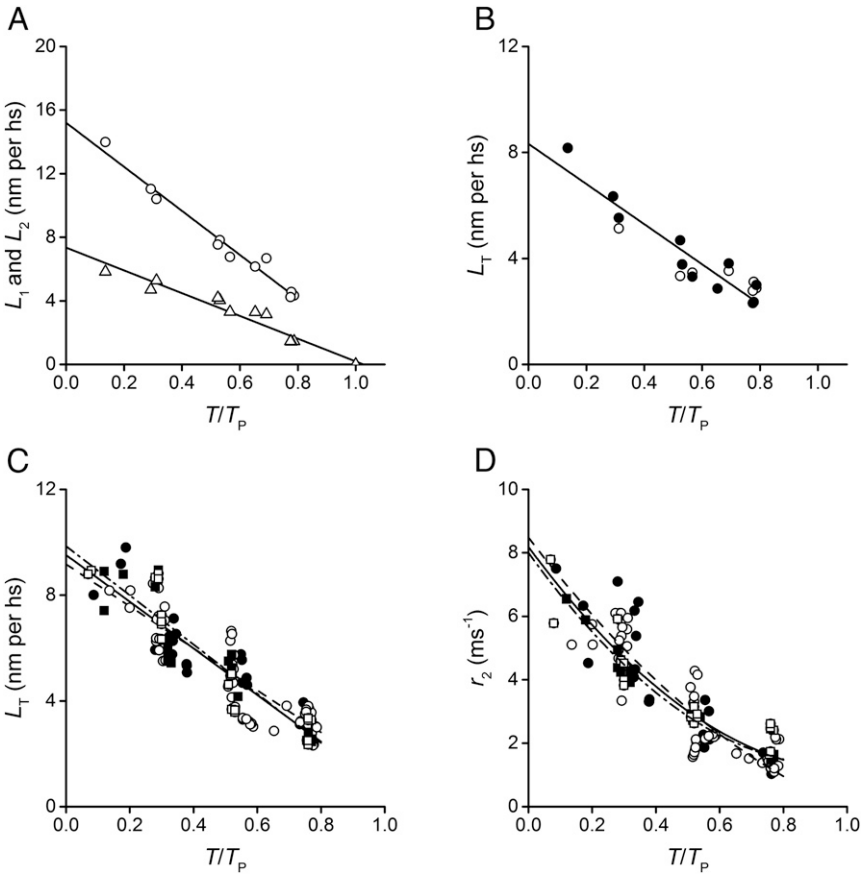

Fig. 3. Force dependence of the parameters of phase 2 velocity transient and effect of changes in SL and Ca^{2+} concentration. (*A*) L_1 relation (triangles) and L_2 relation (circles) at SL of 2.2 μm and 1 mM $[Ca^{2+}]_o$ (pooled data from three trabeculae). Lines are the linear regression fit to data. (*B*) L_T–*T* relation for the same experiments as in *A*, open circles from the striation follower signal, filled circles from the motor position signal. The line is the linear regression fit. (*C*) L_T–*T* relations at different SL and Ca^{2+} concentration. Circles refer to the SL experiments with $[Ca^{2+}]_o$ of 1 mM (open circles, 2.2 μm; filled circles, 1.9 μm), and squares refer to the Ca^{2+} experiments at SL of 2.2 μm (open squares, 1 mM $[Ca^{2+}]_o$; filled squares, 2.5 mM $[Ca^{2+}]_o$). Lines are the linear regression fits to data: continuous, SL of 2.2 μm and 1 mM; dashed, 1.9 μm and 1 mM; dot-dashed, 2.2 μm and 2.5 mM. (*D*) Rate of the isotonic working stroke (r_2) in relation to *T*. Lines are the parabolic fit to data. Symbol and line codes are as in *C*. In all plots, *T* is relative T_P in each condition. Data are mean values ± SEM from eight trabeculae.

(6, 8), the sliding velocity accounted for by the execution of the working stroke is one order of magnitude higher than that accounted for by cyclic ATP-driven actin–myosin interactions during steady shortening (Fig. 4*C*, black open symbols).

The Size and Speed of the Working Stroke Do Not Depend on SL and External Ca^{2+} Concentration. The reduction in SL from 2.2 to 1.9 μm, which reduces T_P from 70 to 30 kPa (circles in Fig. 1*B*), does not affect the size and the rate of the working stroke nor its dependence on *T* relative to T_P at the corresponding SL. L_T– and r_2–*T* relations at SL of 1.9 μm (filled circles in Fig. 3 *C* and *D*, respectively) superimpose on those at SL of 2.2 μm (open circles). The relation between steady shortening velocity and force at SL of 1.9 μm (filled circles in Fig. 4*A*) is shifted below with respect to that determined at 2.2 μm (open symbols), as expected from the effect of SL on T_P. In fact, the parameters of the Hill equation a/T_P (0.39 ± 0.13) and V_0 (8.02 ± 0.76 μm/s per hs) are not significantly different ($P > 0.6$) from those estimated from the data obtained at SL of 2.2 μm and the two relations superimpose when force is plotted relative to T_P at the corresponding SL (Fig. 4*B*). The finding that V_0 is similar at 1.9- and 2.2-μm SL is in agreement with previous work on intact rat trabeculae (13).

The effect of $[Ca^{2+}]_o$ on the isotonic velocity transient was determined in another series of experiments at SL of 2.2 μm. As shown in Fig. 3 *C* and *D*, the increase in $[Ca^{2+}]_o$ from 1 mM (open squares) to 2.5 mM (filled squares), which increases T_P from 66 ± 6 to 99 ± 10 kPa, does not affect the dependence on *T* of either the size (Fig. 3*C*) or the speed (Fig. 3*D*) of the working stroke. The force–velocity relation is shifted above by the increase in $[Ca^{2+}]_o$ (filled squares in Fig. 4*A*), as expected from the effect of $[Ca^{2+}]_o$ on T_P. In fact, when the force is normalized for the corresponding value of T_P, the relations at the two $[Ca^{2+}]_o$ superimpose (Fig. 4*B*). The parameters of the Hill equation a/T_P (0.39 ± 0.06) and V_0 (8.74 ± 0.31 μm/s per hs) are not significantly different ($P > 0.3$) from those estimated with $[Ca^{2+}]_o$ of 1 mM at either 2.2- or 1.9-μm SL. Thus, in agreement with the original work of ter Keurs and collaborators (11, 13, 14), the potentiating effects of the increases of $[Ca^{2+}]_o$ and SL on force appear to act through the same mechanism.

The power at each *T* can be calculated as the product $V \cdot T$. The power–*T* relation with $[Ca^{2+}]_o$ of 1 mM and SL of 2.2 μm (Fig. 4*D*, open symbols, used as the control for the normalization of all *T* values for a unique value of T_P, defined as $T_{P,\ 2.2,\ 1mM}$) shows a maximum at 0.3 peak force. Decrease of SL to 1.9 μm, which reduces the peak force to 0.3 $T_{P,\ 2.2,\ 1mM}$, reduces the maximum power (filled circles), which is still attained at force 0.3 its peak value, to ∼0.3 the maximum power in control, an effect that is fully accounted for by the effect on T_P. Increase of $[Ca^{2+}]_o$ at SL of 2.2 μm from 1 to 2.5 mM, which increases the force peak to 1.5 $T_{P,\ 2.2,\ 1mM}$, increases the maximum power (filled squares),

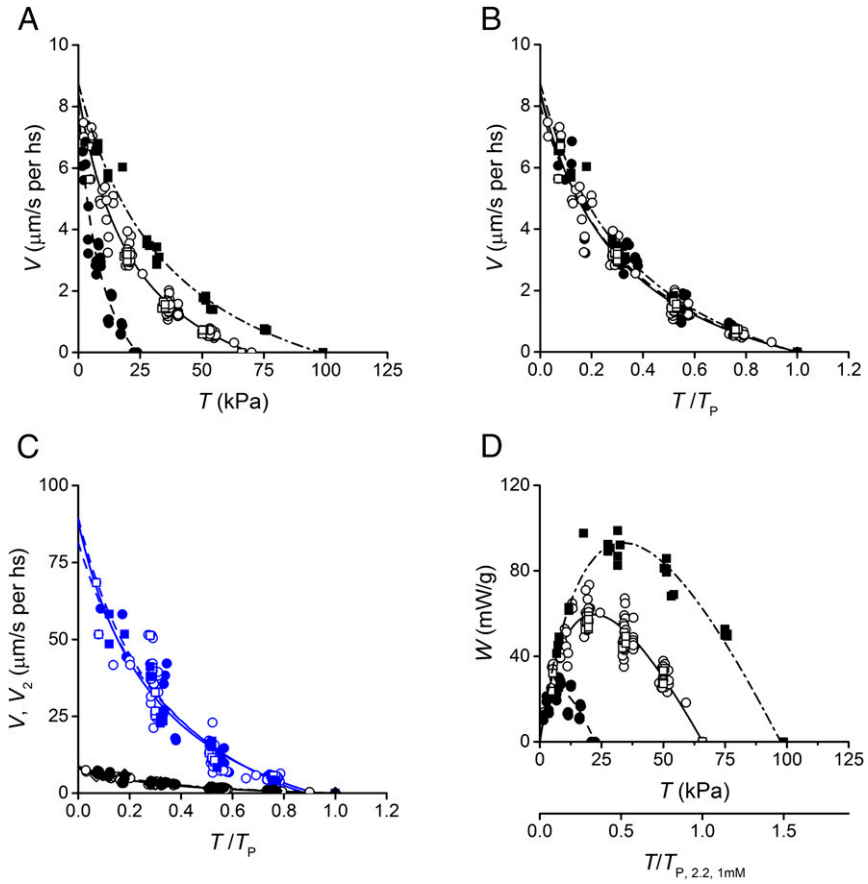

Fig. 4. Force dependence of the parameters of phase 4 of the velocity transient and effect of changes in SL and Ca^{2+} concentration. Symbol and line codes are as in Fig. 3*C*. (*A*) Relation between steady shortening in phase 4 (*V*) and force. (*B*) Same relations as in *A* after normalization of the abscissa for the peak force (T_P) in each condition. (*C*) Comparison between shortening velocity in phase 2 ($V_2 = L_T \cdot r_2$, blue symbols) and in phase 4 (*V*, black symbols) in relation to *T* relative to T_P in each condition. (*D*) Power–force relations calculated from the data in *C*. The lower abscissa is the force in units relative to T_P at SL of 2.2 μm and 1 mM $[Ca^{2+}]_o$ ($T_{P,\ 2.2,\ 1mM}$). Lines in *A*–*C* are the fits to the data using the hyperbolic Hill equation (*Methods*). Lines in *D* are calculated from the lines in *A*. Data are mean values ± SEM from eight trabeculae (the same as in Fig. 3 *C* and *D*).

attained again at force 0.3 its peak value, to 1.5 the maximum power in control.

In conclusion, all of the data reported in Figs. 3 and 4, either transient or steady state, converge to the conclusion that increase of $[Ca^{2+}]_o$ and increase of SL in the range considered increase the isometric force through a common underlying mechanism, which is not related to modulation of the motor mechanokinetic properties but rather to change in the number of active force-generating motors, which is an emergent property of the array arrangement of the motors in the hs.

The Working Stroke of Cardiac Myosin in Situ in Relation to Previous Work. Literature concerning the in situ measurement of the mechanical manifestation of the working stroke of cardiac myosin is scarce (e.g., refs. 15 and 16). In myocytes extracted from the atrium of frog heart, Colomo et al. found that the maximum size of the working stroke, measured by the abscissa intercept of the relation between the force attained during the quick phase of force recovery and the amplitude of the length step (5), is ∼15 nm, a value similar to that estimated here from the ordinate intercept of the L_2 curve in Fig. 3*A*. They determined also the dependence on the size of the length step of the rate of the quick force recovery, which at 10 °C varied with the increase in size of the step release (range, 2–8 nm·hs^{-1}) from ∼500 to ∼2,000 s^{-1}. In this respect, it must be considered that the rate of the working stroke estimated from the early phase of the force recovery following a step is underestimated by any compliance in series with the myosin motors (17, 18). Instead, in the complementary approach of the isotonic velocity transient used in this work, the effect of the series compliance is eliminated and the speed of the early shortening is the direct expression of the rate of the structural change in the myosin motor (7, 8, 18).

We find that, at 27 °C, the size (L_T) and the speed (r_2) of the isotonic working stroke vary from ∼3 nm and 1,000 s^{-1} at high load to ∼8 nm and 6,000 s^{-1} at low load. Comparison of the kinetic values with those obtained for skeletal muscle myosin is not straightforward, due to the much lower temperature used in experiments on skeletal muscle fibers, either intact [frog tibialis anterior, 2–17 °C (8, 9)] or demembranated [rabbit psoas, 12 °C (19)]. Moreover, possible differences in temperature sensitivity between poikilotherms (frog) and homeotherms (mammals) must be taken into account. Therefore, the comparison here is limited to mammalian data. r_2 in the rabbit psoas at 12 °C varies from 1,000 to 8,000 s^{-1} at high and low load, respectively (19). Assuming a Q_{10} of 2.5, r_2 in trabeculae at 12 °C should be at least three times lower than at 27 °C, that is 300 and 2,000 s^{-1} at high and low load, respectively. Thus, the rate of the working stroke estimated from r_2 appears three to four times higher in the fast skeletal myosin from the rabbit than in the cardiac myosin from the rat. This indicates that the cardiac myosin of the rat, even if it is predominantly composed of the fast α-isoform of the myosin heavy chain (MHC) isoform, is slower than the myosin isoform of fast skeletal muscle of the rabbit (MHC 2X). The difference is

even more marked considering that the increase in size across species (rabbit versus rat) is in general expected to be accompanied by slower kinetics (20, 21). This may also provide an explanation for the absence of the phase 3 pause in the isotonic velocity transient of rat trabecula: if the execution of the working stroke at a given load is slower, the subsequent steps consisting of motor detachment, accelerated by the execution of the working stroke, and reattachment further along the actin filament (7) will no longer appear rate limiting for the transition to steady shortening.

As regards the size of the working stroke and its load dependence, comparison of the relations in Fig. 3 *A–C* with the corresponding relations determined in the rabbit psoas (figure 2 *E–G* in ref. 19) makes it evident that the working stroke size is a conserved characteristic across the different myosin isoforms, in agreement with the conclusion of previous in vitro experiments (22, 23).

Perspectives. The application of fast sarcomere-level mechanics to intact trabeculae from rat heart enabled the mechanical and kinetic description of the working stroke of the cardiac myosin in situ, showing that, although the size of the working stroke and its load dependence are quite similar to those of fast skeletal muscle myosin, the working stroke kinetics is slower. Mutations of cardiac myosin have been proposed to be responsible for dilated or hypertrophic cardiomyopathy (1, 2). Studies using in vitro kinetics and mechanics (23, 24) can only define the size of the working stroke and the time the motor remains attached (that is, the reciprocal of the detachment rate) under almost unloaded conditions. The results of our in situ study demonstrate that this approach is the only one able to quantitatively describe the mechanokinetic properties of the motor, providing a powerful new tool for defining the mechanism of the cardiomyopathy-causing mutations in cardiac myosin and for testing specific therapeutic interventions.

Methods

Sample Preparation and Mechanical Setup. Thin, unbranched uniform cardiac trabeculae were dissected from the right ventricle from male Wistar rats (weighing 230–280 g) in agreement with the Italian regulation on animal experimentation (Authorization 956/2015-PR in compliance with Decreto legislativo 26/2014) and transferred into a thermoregulated trough perfused with a modified Krebs–Henseleit solution equilibrated with carbogen (95% O_2, 5% CO_2) for attachment via titanium double hooks to the lever arms of a capacitance gauge force transducer and a motor servosystem. The temperature of the solution was maintained at 27 °C. The SL was set at 2.2 μm at rest, and the length of the trabecula (L_0) was measured. A striation follower was used to record SL changes in a 0.7- to 1.5-mm segment across the central region of the preparation (10). Force, motor lever position, SL, and stimulus signals were recorded with a multifunction I/O board (National Instruments; PCI-6110E).

Experimental Protocol and Data Analysis. Trabeculae were electrically stimulated at 0.5 Hz to produce twitches. An iterative feedforward method was used to keep SL constant during systole until the final part of force relaxation (Fig. 1*A*). When the force had attained 95% of the peak (T_P), the control was switched from fixed-end mode to force-clamp mode and 1 ms later a step in force (rise time ∼200 μs) to a fraction of T_P (range 0.2–0.9 T_P) was imposed to elicit the isotonic velocity transient, until a preset shortening level was reached (Fig. 2 *A* and *B*). The protocol was repeated at two SLs (1.9 and 2.2 μm) and at two $[Ca^{2+}]_o$ (1.0 and 2.5 mM). Force is expressed as force per cross-sectional area of the preparation (in kilopascals). A dedicated program written in LabVIEW (National Instruments) and Origin 2015 (OriginLab Corporation) was used for analysis.

The force–velocity data are fitted with the hyperbolic Hill equation (25):

$$(T + a)(V + b) = (V_0 + b)a,$$

where a and b are the distances between the asymptotes and the ordinate and abscissa axes, and V_0 (the ordinate intercept) estimates the unloaded shortening velocity. The power output (W) at any force is calculated by the product between force and velocity. Data are expressed as mean ± SEM unless differently specified. An expanded version of *Methods* is given in *SI Methods*. Source mechanical data can be found in Dataset S1.

ACKNOWLEDGMENTS. We thank Mario Dolfi for skilled technical assistance. This work was supported by MIUR-PRIN Project 2010R8JK2X (Italy), Ente Cassa di Risparmio di Firenze Project 2012.0611 (Italy), and Telethon Project GGP12282 (Italy).

1. Spudich JA (2014) Hypertrophic and dilated cardiomyopathy: Four decades of basic research on muscle lead to potential therapeutic approaches to these devastating genetic diseases. *Biophys J* 106(6):1236–1249.
2. Moore JR, Leinwand L, Warshaw DM (2012) Understanding cardiomyopathy phenotypes based on the functional impact of mutations in the myosin motor. *Circ Res* 111(3):375–385.
3. Marston SB (2011) How do mutations in contractile proteins cause the primary familial cardiomyopathies? *J Cardiovasc Transl Res* 4(3):245–255.
4. Aksel T, Choe Yu E, Sutton S, Ruppel KM, Spudich JA (2015) Ensemble force changes that result from human cardiac myosin mutations and a small-molecule effector. *Cell Rep* 11(6):910–920.
5. Huxley AF, Simmons RM (1971) Proposed mechanism of force generation in striated muscle. *Nature* 233(5321):533–538.
6. Piazzesi G, et al. (2007) Skeletal muscle performance determined by modulation of number of myosin motors rather than motor force or stroke size. *Cell* 131(4):784–795.
7. Reconditi M, et al. (2004) The myosin motor in muscle generates a smaller and slower working stroke at higher load. *Nature* 428(6982):578–581.
8. Piazzesi G, Lucii L, Lombardi V (2002) The size and the speed of the working stroke of muscle myosin and its dependence on the force. *J Physiol* 545(Pt 1):145–151.
9. Decostre V, Bianco P, Lombardi V, Piazzesi G (2005) Effect of temperature on the working stroke of muscle myosin. *Proc Natl Acad Sci USA* 102(39):13927–13932.
10. Huxley AF, Lombardi V, Peachey D (1981) A system for fast recording of longitudinal displacement of a striated muscle fibre. *J Physiol* 317:12–13.
11. ter Keurs HE, Rijnsburger WH, van Heuningen R, Nagelsmit MJ (1980) Tension development and sarcomere length in rat cardiac trabeculae. Evidence of length-dependent activation. *Circ Res* 46(5):703–714.
12. Huxley AF (1974) Muscular contraction. *J Physiol* 243(1):1–43.
13. Daniels M, Noble MI, ter Keurs HE, Wohlfart B (1984) Velocity of sarcomere shortening in rat cardiac muscle: Relationship to force, sarcomere length, calcium and time. *J Physiol* 355:367–381.
14. de Tombe PP, ter Keurs HE (1992) An internal viscous element limits unloaded velocity of sarcomere shortening in rat myocardium. *J Physiol* 454:619–642.
15. Colomo F, Poggesi C, Tesi C (1994) Force responses to rapid length changes in single intact cells from frog heart. *J Physiol* 475(2):347–350.
16. De Winkel ME, Blangé T, Treijtel BW (1995) Viscoelastic properties of cross bridges in cardiac muscle. *Am J Physiol* 268(3 Pt 2):H987–H998.
17. Linari M, Piazzesi G, Lombardi V (2009) The effect of myofilament compliance on kinetics of force generation by myosin motors in muscle. *Biophys J* 96(2):583–592.
18. Piazzesi G, et al. (2014) The myofilament elasticity and its effect on kinetics of force generation by the myosin motor. *Arch Biochem Biophys* 552-553:108–116.
19. Caremani M, Melli L, Dolfi M, Lombardi V, Linari M (2013) The working stroke of the myosin II motor in muscle is not tightly coupled to release of orthophosphate from its active site. *J Physiol* 591(20):5187–5205.
20. Pellegrino MA, et al. (2003) Orthologous myosin isoforms and scaling of shortening velocity with body size in mouse, rat, rabbit and human muscles. *J Physiol* 546(Pt 3): 677–689.
21. Andruchov O, Wang Y, Andruchova O, Galler S (2004) Functional properties of skinned rabbit skeletal and cardiac muscle preparations containing alpha-cardiac myosin heavy chain. *Pflugers Arch* 448(1):44–53.
22. Palmiter KA, Tyska MJ, Dupuis DE, Alpert NR, Warshaw DM (1999) Kinetic differences at the single molecule level account for the functional diversity of rabbit cardiac myosin isoforms. *J Physiol* 519(Pt 3):669–678.
23. Tyska MJ, Warshaw DM (2002) The myosin power stroke. *Cell Motil Cytoskeleton* 51(1):1–15.
24. Alpert NR, et al. (2002) Molecular mechanics of mouse cardiac myosin isoforms. *Am J Physiol Heart Circ Physiol* 283(4):H1446–H1454.
25. Hill AV (1938) The heat of shortening and the dynamic constants of muscle. *Proc R Soc Lond B Biol Sci* 126:136–195.
26. Mulieri LA, Hasenfuss G, Ittleman F, Blanchard EM, Alpert NR (1989) Protection of human left ventricular myocardium from cutting injury with 2,3-butanedione monoxime. *Circ Res* 65(5):1441–1449.
27. Lombardi V, Piazzesi G (1990) The contractile response during steady lengthening of stimulated frog muscle fibres. *J Physiol* 431:141–171.